

SECONDARY KELVIN-HELMHOLTZ INSTABILITY IN A 3D STABLY STRATIFIED TEMPORAL MIXING LAYER BY DIRECT NUMERICAL SIMULATION

Denise M. V. Martinez^a, Edith B. C. Schettini^b and Jorge H. Silvestrini^c

^a *Departamento de Matemática, Fundação Universidade Federal do Rio Grande - FURG, Av. Itália, Km 8 - 962001-900, Rio Grande, RS, Brazil, denisevmartinez@yahoo.com.br*

^b *Instituto de Pesquisas Hidráulicas, Universidade Federal do Rio Grande do Sul - UFRGS, Av. Bento Gonçalves, 9500 - 91501-970 - Porto Alegre, RS, Brazil, bcamano@iph.ufrgs.br*

^c *Departamento de Engenharia Mecânica e Mecatrônica, Pontifícia Universidade Católica do Rio Grande do Sul - PUCRS, Av. Ipiranga, 6681 - 90619-900 - Porto Alegre, RS, Brasil, jorgehs@pucrs.br*

Keywords: Direct numerical simulation, secondary instability, stable stratification, baroclinic layer.

Abstract. The present work investigates the nature of the transition to turbulence in the stably stratified mixing layer, which is a complex process with great importance for geophysical and industrial flows. In the stably stratified mixing layer, the streamwise density gradient, which corresponds to the spanwise component of the baroclinic torque in the Boussinesq approximation, feeds the region between the Kelvin-Helmholtz (KH) vortices with vorticity and forms a thin vorticity layer, called baroclinic layer. The competition between buoyancy and inertial forces modifies the dynamics of this layer. As consequence, two different secondary instabilities are found to develop upon the baroclinic layer: one originated near the core region of the KH vortex, called near-core instability, that propagates towards the baroclinic layer and the other of Kelvin-Helmholtz type developed in the baroclinic layer itself. The development of these instabilities in the baroclinic layer depends on the Richardson number, the Reynolds number and the initial conditions. The main objective of this paper is to investigate the occurrence of secondary instabilities in the baroclinic layer of a three-dimensional stably stratified mixing layer using Direct Numerical Simulation (DNS). The development of streamwise vortices and its interactions with the secondary KH structures are focused. Typical Richardson numbers ranging from 0.07 to 0.167 are considered while the Reynolds number is kept constant (500 or 1000). White noise and forced perturbation are used as initial conditions. The Navier-Stokes equations, in the Boussinesq approximation, are solved numerically using a sixth-order compact finite difference scheme to compute the spatial derivatives, while the time integration is performed with a third-order low-storage Runge-Kutta method. The numerical results show the development of a jet in the baroclinic layer adjacent to vorticity layers of opposite signs. These layers are created baroclinically by convective motions inside the primary KH vortex and amplifies the near-core instability. It is shown that this instability appears due to the formation of a negative vorticity layer generated between two co-rotating positive vortices. The negative vorticity layer unstables the baroclinic layer and forms small vortices of the KH type. The intensity of the negative vorticity layer depends on the Richardson and Reynolds numbers and defines occurrence or not of secondary KH structures. Interactions between these secondary KH structures and streamwise vortices are also observed. They strongly depend on the initial conditions.

1 INTRODUCTION

The dynamics of the stably stratified mixing layer, mainly its transition to turbulence, is a problem of considerable interest in fluid dynamics with applications in both geophysical sciences and engineering. The turbulence prevails in most flows of practical interest and may strongly affect important global features of these flows. Thus, the precise description of the instabilities that occur during the transition to turbulence and their reliable prediction are matters of primary concern in the study of a mixing layer. Recently, Direct Numerical Simulations (DNS) have added considerably to our understanding of the dynamics of a mixing layer, since they solve entirely all the spatial and temporal scales of the flow (Caulfield and Peltier, 2000; Cortesi et al., 1998; Staquet, 1995; Smyth, 2003).

The stably stratified mixing layer develops at the interface of two parallel streams of fluid moving horizontally at different velocities, having different densities, the upper stream being lighter than the lower one.

Miles (1961) and Howard (1961), based on a linear stability analysis, showed that for the Kelvin-Helmholtz (KH) instability to occur in the stratified mixing layer from an infinitely small disturbance, the Richardson number should be less than 0.25 somewhere within the flow. This first instability that occurs in the mixing layer is due to the inflectional nature of the velocity profile (Michalke (1964)).

In the stably stratified mixing layer occurs a streamwise density gradient ($\partial\rho/\partial x$) that corresponds to the spanwise component of the baroclinic torque in the Boussinesq approximation. This streamwise density gradient feeds the region between the KH vortices with vorticity and forms thin vorticity layers there.

The vorticity layer, which is formed under the action of the buoyancy effects and strains between the billows of the KH, was defined as a baroclinic layer by Staquet (1995) and identified by Caulfield and Peltier (2000). This baroclinic layer, subject to baroclinic vorticity production, is continuously stretched, admitting a strain rate roughly proportional to the circulation around the cores (Corcos and Sherman, 1976). The development of the secondary instabilities in the baroclinic layer depends on the stratification degree of the flow (characterized by the Richardson number, Ri), on the Reynolds number (Re) and on the imposed initial conditions.

Evidence of the occurrence of secondary KH instability in a baroclinic layer was reported in geophysical flows for the atmosphere (Gossard et al., 1970) and in the ocean (Haury et al., 1979), in a very few laboratory experiments (Atsavapranee and Gharib, 1997; Altman, 1988; Thorpe, 1985) and through numerical simulation (Staquet, 1995, 2000; Smyth, 2003; Martinez, 2006; Martinez et al., 2005).

The main objective of this paper is to investigate the occurrence of secondary instabilities in the baroclinic layer of a three-dimensional stably stratified mixing layer using DNS. The purpose is also to verify the influence of the secondary KH instability in the three-dimensionalization of the flow. Typical Richardson numbers ranging from 0.07 to 0.167 are considered while the Reynolds number is kept constant and equal to 500 or 1000. Two different secondary instabilities are found in the baroclinic layer: one is originated near the core region of the KH vortex, called near-core instability, which propagates towards the baroclinic layer, another one of KH type in the baroclinic layer itself.

The near-core instability (Staquet, 1995) is developed near the unstable regions of the primary KH vortex. This instability appears due to negative vorticity (correspond to the blue color in the Figure 1) generated between two co-rotating vortices, formed by baroclinic layer of positive vorticity (red color) and the core of the primary KH vortex, by strong streamwise density

gradient. The negative vorticity layer unstabilizes the baroclinic layer and makes it becomes similar to a mixing layer. The new mixing layer, when unstable, forms small vortices of the KH type with the same dynamics as the primary KH vortices, as shows the Figure 1.

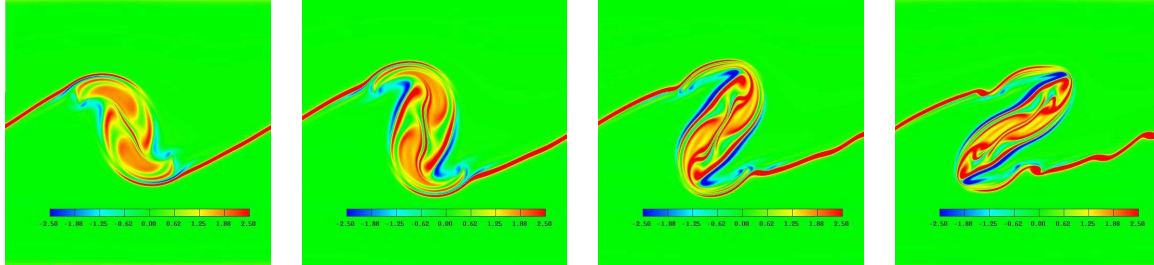


Figure 1: Development of the secondary near-core instability and secondary KH instability in the baroclinic layer. Simulation 2D in a computational grid of $768 \times 1 \times 961$ points for $Re = 2000$ and $Ri = 0.167$.

In previous simulations (Martinez et al., 2004; Martinez, 2006), at lower values of Re (< 500), was observed the formation of the baroclinic layer, but without manifestation of the secondary KH instability. The occurrence of the secondary KH instability in the baroclinic layer of a 2D stably stratified mixing layer, for different Reynolds numbers (500, 1000, 2000), was clearly demonstrated using DNS by Martinez et al. (2005) and Martinez (2006). In these works were verified that the production of negative vorticity inside the vortex core is fundamental for generation of secondary vortices of the KH type. The related works had shown that the production of negative vorticity in the vortex core is rapidly followed by the growth of the secondary KH instability in the baroclinic layer; moreover, this instability does not develop if the negative vorticity is too low compared to the positive one (this instability is referred to as the near-core instability). In 2D simulations at $Re = 500$, the secondary KH instability appeared both at $Ri = 0.07$ (weak stratification) and at $Ri = 0.167$ (strong stratification). This fact is not reported by Staquet (1995), which showed that the near-core instability amplify in the baroclinic layer only for $Re \geq 1500$, but it is possible the amplification of the secondary KH instability for $Re \geq 400$ when $Ri = 0.167$. Smyth (2003) showed that the secondary KH instability can be developed without the occurrence of the near-core instability in a unstable stratified mixing layer, for high Reynolds numbers. However, the following doubt comes up: How does the secondary KH instability compete with the 3D instabilities?

2 MATHEMATICAL MODEL AND NUMERICAL METHOD

2.1 Governing Equations

The basic governing equations in dimensionless form for mass conservation, Navier-Stokes in the Boussinesq approximation, and energy equation, in a Cartesian frame of reference $\mathfrak{R} = (0; x, y, z)$ are:

$$\vec{\nabla} \cdot \vec{u} = 0, \tag{1}$$

$$\frac{\partial \vec{u}}{\partial t} = -\vec{\nabla} P - \vec{\omega} \times \vec{u} - Ri \rho \vec{i}_z + \frac{1}{Re} \nabla^2 \vec{u}, \tag{2}$$

$$\frac{\partial \rho}{\partial t} + \vec{u} \cdot \vec{\nabla} \rho = \frac{1}{RePr} \nabla^2 \rho. \tag{3}$$

where $P(x, y, z, t)$ is the modified pressure field, $\rho(x, y, z, t)$ is density or active scalar, $\vec{u}(x, y, z, t)$ is the velocity field and $om\vec{e}ga$ is the vorticity field. There are two dimensionless relevant parameters: the Reynolds number $Re = U\delta_i/\nu$ based on the half velocity difference across the shear layer (U) and on the initial vorticity thickness defined by $\delta_i = 2U/(du/dz)_{max}$, and the Richardson number $Ri = g\Delta\rho R\delta_i/\rho_0 U^2$, where $\Delta\rho R$ is density scale and R is the ratio of initial vorticity thickness and the density thickness. The time is made dimensionless using the advective scale δ_i/U .

In these equation, the scales of length, velocity and density are such as $\delta_i = 1$, $U = 1$ and $\Delta\rho = 1/R$. In this manner, $Re = 1/\nu$ and $Ri = g/\rho_0$. At $t = 0$, $\rho_0(x, y, z, t = 0) = \rho_0 + \rho(z)$, where ρ_0 is a constant density reference and $\rho(z)$ is the basic density profile.

2.2 Initial and boundary conditions

The initial conditions are defined in terms of velocity and density fields as:

$$u(z, t = 0) = U \operatorname{erf} \left(\frac{\sqrt{\pi} z}{\delta_i} \right) \quad (4)$$

$$\rho(z, t = 0) = -\frac{1}{R} \operatorname{erf} \left(\frac{\sqrt{\pi} R z}{\delta_i} \right). \quad (5)$$

With the objective to promote the development the KH instability and to unchain the formation of the KH billows, a field of perturbations was added to the basic velocity profile. This field is composed by two waves corresponding to the most amplified wave number (α_a) and its fifth sub-harmonic ($\alpha_a/2$), and a white noise in spanwise direction. The associated most unstable wavelength given by linear stability theory is approximately $\lambda_a = 7\delta_i$ where the most amplified wave number $\alpha_a = 2\pi/\lambda_a$ being $0.889\delta_i^{-1}$ (Michalke, 1964). These perturbations promote, respectively, the development of the KH instability, the pairing process and the formation of streamwise vortices. In the present case, no density fluctuation is superimposed upon $\rho(z)$ at $t = 0$.

The boundary conditions for the temporal mixing layer are:
 periodic: used in the streamwise (x) and spanwise (y) directions; and
 free-slip: used in the vertical direction (z). This condition imposes the following restrictions: $\frac{\partial u}{\partial z} = \frac{\partial v}{\partial z} = 0$ and $w = 0$ for $z = \pm \frac{Lz}{2}$.

2.3 Numerical Method

Equations (1) to (3) are solved numerically, in the domain shown in Figure 2, using a sixth-order compact finite difference scheme (Lele, 1992) to evaluate spatial derivatives. The compact schemes are implicit ones that relate the value of the derivative in a point to the value of the derivative in neighboring points. For the spatial discretization considering a uniform mesh, where the independent variable for each node i is $\xi_i = (i-1)\Delta\xi$, $1 \leq i \leq N$ and $\xi = x, y$ or z , the function values for nodes are $f_i = f(\xi_i)$ and first derivative $f'_i = f'(\xi_i)$, is given by:

$$\alpha f'_{i-1} + f'_i + \alpha f'_{i+1} = a \frac{f_{i+1} - f_{i-1}}{2\Delta\xi} + b \frac{f_{i+2} - f_{i-2}}{4\Delta\xi}. \quad (6)$$

The second derivative is given by:

$$\alpha f''_{i-1} + f''_i + \alpha f''_{i+1} = a \frac{f_{i+1} - 2f_i + f_{i-1}}{\Delta\xi^2} + b \frac{f_{i+2} - 2f_i + f_{i-2}}{4\Delta\xi^2}. \quad (7)$$

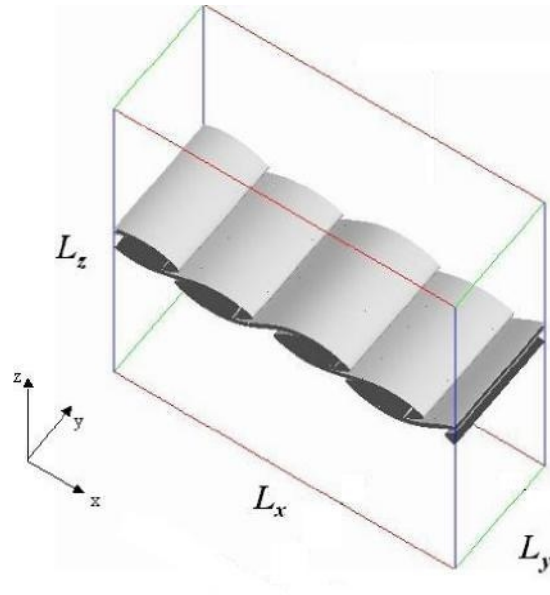


Figure 2: Schematic view of domain.

The sixth order is obtained with the set of parameters (Lele, 1992) :

$$\alpha = \frac{1}{3}, \quad a = \frac{14}{9}, \quad b = \frac{1}{9} \quad \text{for Eq.(6),}$$

$$\alpha = \frac{2}{11}, \quad a = \frac{12}{11}, \quad b = \frac{3}{11} \quad \text{for Eq.(7).}$$

Equations (6) and (7) are valid for three spatial directions (x, y, z) in all the mesh points.

The time integration is performed with a third-order low-storage Runge-Kutta method (Williamson, 1980). The integration of Eq.(2) at times t^n and $t^{(n+1)}$ is performed through 3 fractional time step $p = 0, 1, 2$, where $\vec{u}^{(0)} = \vec{u}^{(n)}$ and $\vec{u}^{(3)} = \vec{u}^{(n+1)}$,

$$\frac{u^{(p+1)} - u^{(p)}}{\Delta t} = \alpha_p F^{(p)} + \beta_p F^{(p-1)} - \vec{\nabla} \Pi^{(p+1)} \tag{8}$$

$$\vec{\nabla} \cdot \vec{u}^{p+1} = 0, \tag{9}$$

where

$$\vec{F} = -\vec{\omega} \times \vec{u} - Ri \rho \vec{i}_z + \frac{1}{Re} \nabla^2 \vec{u}, \tag{10}$$

$$\Pi^{(p+1)} = \frac{1}{\Delta t} \int_{t_n}^{t^{(n+1)}} P dt, \tag{11}$$

and α_p, β_p are coefficients to each fractional step p , given by Williamson (1980):

$$\alpha_0 = \frac{8}{15}, \quad \beta_0 = 0; \quad \alpha_1 = \frac{5}{12}, \quad \beta_1 = \frac{-17}{60}; \quad \alpha_2 = \frac{3}{4}, \quad \beta_2 = \frac{-5}{12}.$$

The Eq.(8) can be split into two steps,

$$\frac{\vec{u}^* - u^{(p)}}{\Delta t} = \alpha_p F^{(p)} + \beta F^{(p-1)}, \tag{12}$$

$$\frac{\vec{u}^{(p+1)} - \vec{u}^*}{\Delta t} = -\vec{\nabla}\Pi^{(p+1)}. \quad (13)$$

In this conventional fractional method, step $p + 1$ is obtained by solving the Poisson equation. Thus the incompressibility condition is ensure,

$$\vec{\nabla} \cdot \vec{\nabla}\Pi^{(p+1)} = \frac{\vec{\nabla} \cdot \vec{u}^*}{\Delta t}. \quad (14)$$

More details about the numerical code can be found in [Lardeau et al. \(2002\)](#) and [Silvestrini and Lamballais \(2002\)](#). Equation (3) is solved in the same way as Eq.(2) by making,

$$\frac{\rho^{(p+1)} - \rho^{(p)}}{\Delta t} = \alpha_p \vec{G}^{(p)} + \beta_p G^{(p-1)}, \quad (15)$$

where

$$\vec{G} = -\vec{u} \cdot \vec{\nabla}\rho + \frac{1}{RePr} \nabla^2 \rho.$$

3 CODE VALIDATION AND AMPLIFICATION RATE

In order to validate the numerical code the evolution of a small disturbance was considered in a 2D domain. The results were compared with the linear stability theory, where the disturbance is described by the Taylor-Goldstein equation ([Hazel, 1972](#)).

The computational domain used is a square of side $L = 7\delta_i$, corresponding to the most amplified wave number $\alpha_a = 0.889\delta_i^{-1}$ given by linear stability theory. The Reynolds number is 300, the Prandtl number is 1 and the Richardson number tested are 0.0, 0.1 and 0.2. The initial amplitude of the perturbation was $10^{-6}U$.

Tests with different computational grid of $n_x \times n_z$ points were done (see Table 1). As expected, the grid size has a great influence over the amplification rate. In the test with a

Ri	$N1$ 64 × 65	$N2$ 64 × 129	$N3$ 128 × 129	Ref.Value Hazel,1972
0	0.18732	0.18632	0.1861	0.1867
0.1	0.19492	0.17057	0.1650	0.1594
0.2	0.13597	0.16532	0.1329	0.1259

Table 1: Comparison of amplification rate with the reference value for different grids.

computational grid of $N2 = 64 \times 129$ points, it was noticed that the streamwise resolution interferes in the evolution of the wave amplitude (stratified case), when comparing with grid $N1$ (see Table 1). Thus, for the stratified case ($Ri = 0.1$) the grid $N2$ showed a decrease of the amplification rate due to the increase in the vertical resolution, with an error of the 7% in relation to the reference value, whereas for $Ri = 0.2$ there is an increase in the amplification rate. Probably this occurs because the streamwise density gradient is not being well solved.

Figure 3 shows the time evolution of the amplitude for different Richardson numbers (0; 0.1; 0.2) obtained from the simulation with grid $N3 = 128 \times 129$ points. Clearly, there is a region of exponential amplification, which corresponds to regime governed by the linear theory. In this test, the errors found are of -0.32% for $Ri = 0$, 3.5% for $Ri = 0.1$ and 10.2% for $Ri = 0.2$. The comparison of the simulation $N3$ with the numerical results of [Hazel \(1972\)](#), shown in Table 1, gives good agreement for the temporal growth rates the stably stratified mixing layer.

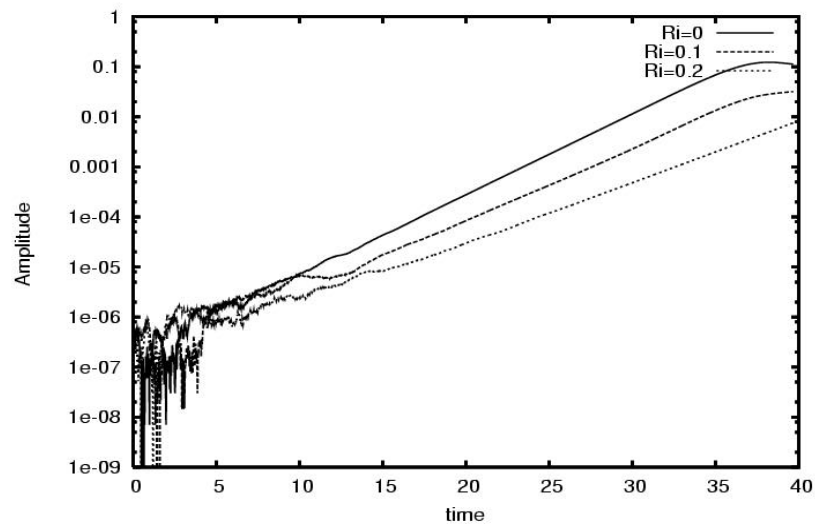


Figure 3: Amplitude evolution for simulation N3.

4 PHYSICAL AND COMPUTATIONAL PARAMETERS

The computational parameters for the simulations are given in Table 2. The parameter ε_i denotes the amplitude of the perturbation superimposed on the basic velocity profile for the fundamental ($i = 1$), the first sub-harmonic ($i = 2$) and for the spanwise mode ($i = 3$), respectively. The random component of the initial condition for the spanwise velocity fluctuation (v') is composed of small amplitude white noise.

Simulation	Re	R_i	Domain (L_x, L_y, L_z)	Grid ($n_x \times n_y \times n_z$)	Forcing ($\varepsilon_1, \varepsilon_2, \varepsilon_3$)
3DI	500	0.07	(14, 5, 14)	512 × 32 × 513	(1%U; 0.1%U; white noise)
3DII	500	0.167	(14, 5, 14)	512 × 32 × 513	(1%U; 0.1%U; white noise)
3DIII	1000	0.07	(14, 5, 14)	512 × 32 × 513	(1%U; 0.1%U; white noise)

Table 2: Physical and computational parameters.

5 INFLUENCE OF THE SECONDARY KELVIN-HELMHOLTZ INSTABILITY IN THE TRANSITION TO TURBULENCE

Simulations of pairing process of the KH billows in stratified flow (Smyth, 1999) show strong three-dimensional motions developing in the cores during pairing, while the region between vortices remain two-dimensional. However, the 3D process is sensitive to the form of the initial perturbations (Cortesi et al., 1998).

In stratified mixing layer the 3D process is complex due to the greater number of secondary instabilities that propagate in the flow. The instabilities that developed in a 3D stably stratified mixing layer may be divided in two groups: one that grows within the vortex core and the other that develops in the region between the cores (Martinez et al., 2006). Within the cores two types of instabilities are found. The one found by Pierrehumbert and Widnall (1982), that does not depend upon the buoyancy effects, called translative instability, and the gravitational convective instability that is driven by buoyancy effects (Showalter et al., 1994).

The near-core instability, discovered by Staquet (1995), would be located close to the place where the secondary gravitational convective instability develops. In the region between the cores two types of instabilities are found: the secondary shear instability, predicted by Klaassen and Peltier (1991), and the secondary KH instability (Staquet, 1995), which depends on the stratification degree of the flow (Ri) and on the Reynolds number (Re). In this section it is verified qualitatively the way that the secondary KH instability affects 3D process and the formation of the streamwise vortices.

5.1 Dependence on the Richardson and Reynolds numbers

The Reynolds and Richardson numbers are parameters that govern the evolution of the primary instability and secondary instability of the KH type in the stably stratified mixing layer. In previous simulations were verified that when there is a pairing of the simulated vortices both the near-core and the secondary KH instabilities are able to grow upon the baroclinic layer.

Figure 4 shows results obtained for $Re = 500$ and $Ri = 0.167$, in a domain configuration of $(L_x, L_y, L_z) = (14, 5, 14)$, using a small white noise in the initial condition for the perturbation velocity field in the spanwise direction whereas for the others the forced condition.

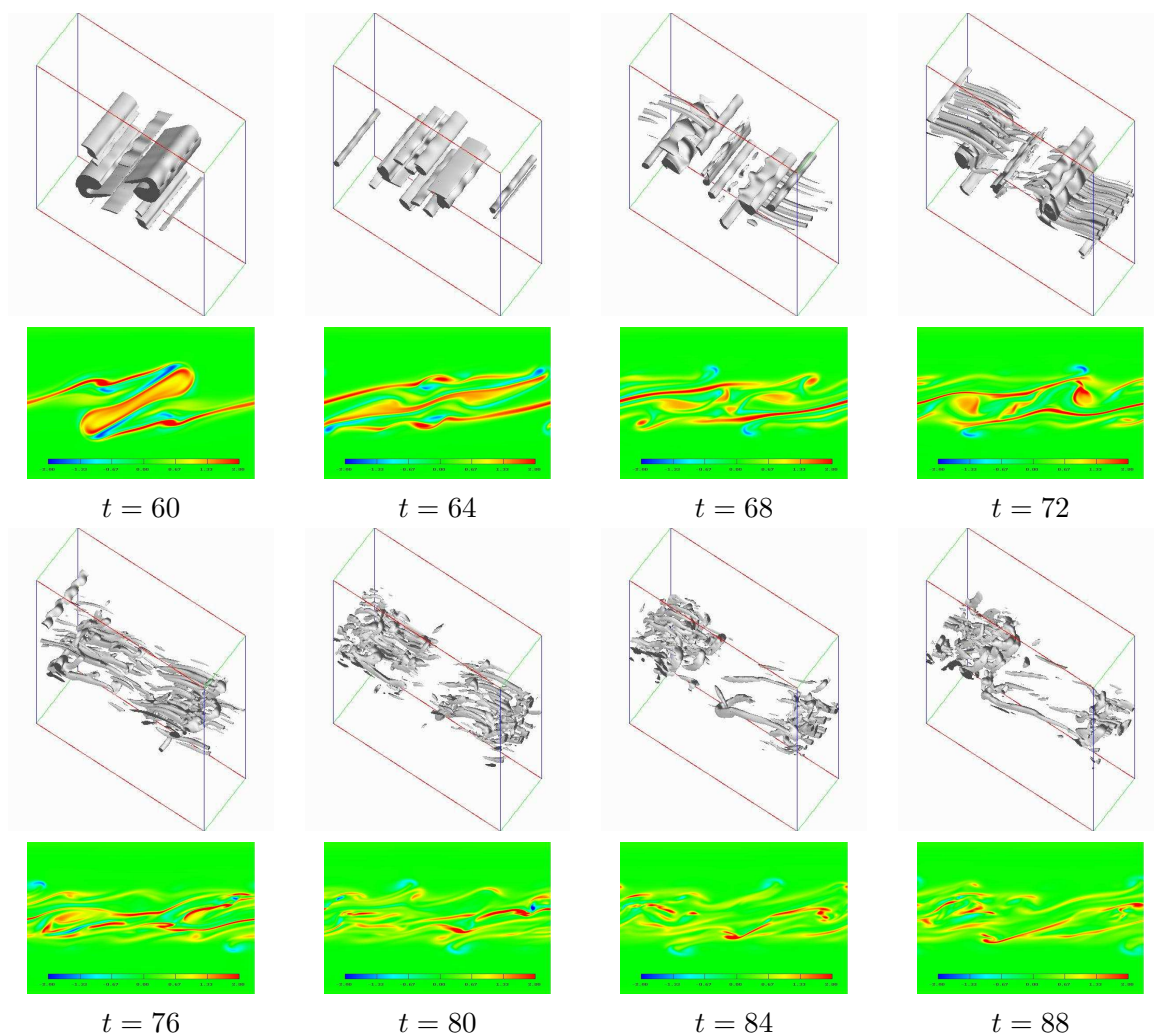


Figure 4: Isosurfaces of $Q = 0.2$ and streamwise cross-sectional plots of spanwise vorticity. Simulation 3DII, $Re = 500$, $Ri = 0.167$.

The streamwise vortices are developed after the saturation of the primary vortices of KH in unstratified case. When the secondary KH instability develops upon the baroclinic layer of the stably stratified mixing layer, as shown in the Figure 4, the streamwise vortices can be visualized after the saturation of the secondary KH vortices.

The Figure shows isosurfaces using the Q-criterion and streamwise cross-sectional plots of spanwise vorticity for different times. In this simulation it was verified that the secondary KH instability is of two-dimensional nature (Figure 4, $t = 60 - 64$), through successive cross-sectional plots of spanwise vorticity. Figure 4 shows that the secondary KH vortices have the same dynamics that the primary KH vortices ($t = 64$) even when the flow is 3D.

Figure 5, for $Ri = 0.07$, shows that the secondary KH instability appears with lesser intensity that for $Ri = 0.167$. The secondary KH instability does not develop as in the case of strong stratification, possibly because the vorticity of the baroclinic layer and the adjacent layer of negative vorticity are too weak to allow the development of this instability. Thus the responsible mechanism for the generation or local destruction of vorticity becomes weakened and as consequence the streamwise vortices are not formed.

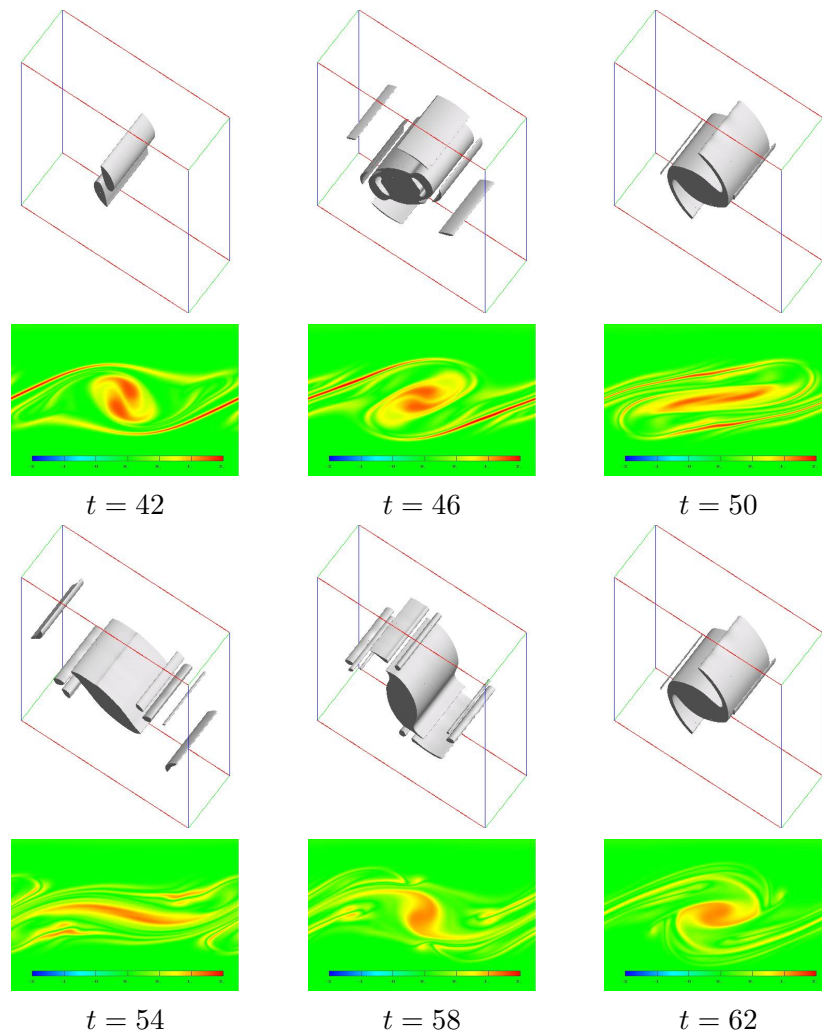


Figure 5: Isosurfaces of $Q = 0.2$ and streamwise cross-sectional plots of spanwise vorticity. Simulation 3DI, $Re = 500$, $Ri = 0.07$.

In Figure 6, it is observed the temporal evolution of the positive and negative vorticities (ω_y)

for simulations 3DI and 3DII. It can be noticed that the vorticity at $Ri = 0.167$ increases beyond the initial value and, after the pairing process ($t \geq 28$) a negative vorticity decrease, presenting a symmetry in relation with the positive vorticity. It is observed that the secondary KH instability developed in the flow if the negative vorticity is of comparable value with the positive one. This fact makes possible the successive secondary KH vortices displayed in the flow, permitting the existence of a baroclinic layer of higher vorticity than the maximum initial vorticity, as well as the generation of negative vorticity. This non-conservation of the local vorticity is also a fundamental feature of three-dimensional turbulent flows. The maximum vorticity of the flow for $Ri = 0.167$ is reached at time equal 80 when the flow has become turbulent. The Reynolds number has influence on the development of the secondary KH instability and

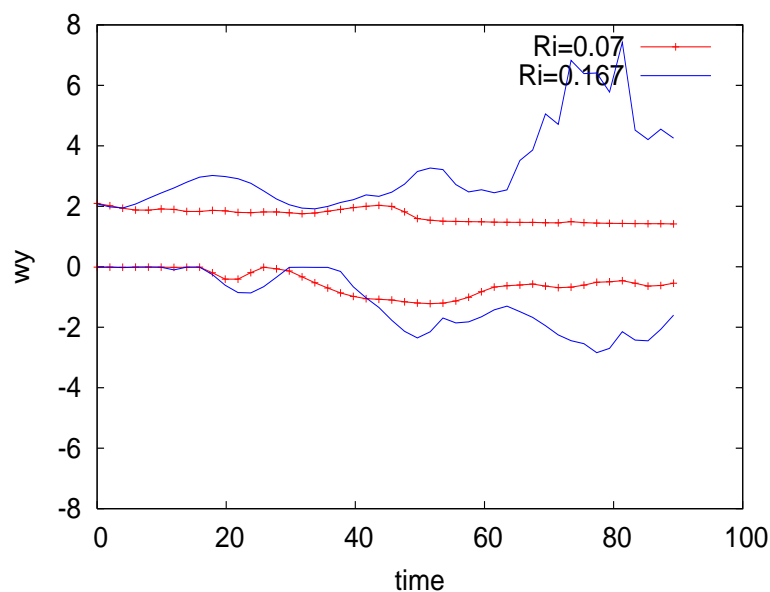


Figure 6: Temporal evolution of the maximum and minimum vorticity (ω_y), for $Ri = 0.07$ and $Ri = 0.167$ ($Re = 500$), simulation 3DI and 3DII, respectively.

formation of the streamwise vortices, as it is verified in Figure 7 for $Ri = 0.07$ and $Re = 1000$.

The precise numerical treatment of the turbulence requires that the entire band of scales which ranges from the energy-carrying to the dissipative motions is resolved in time and space. Figure 8 shows the spectrum of kinetic energy in function of the streamwise wavenumber at different times, for $Ri = 0.07$ and $Ri = 0.167$ and $Re = 500$.

It is seen that the energy spectrum takes its maximum within the low-wavenumber regime, while it shows behavior turbulent in high-wavenumber. This spectrum suggests a mechanism of transference of energy towards dissipative scales. The peak in the time $t = 2$ corresponds to the most amplified wavenumber, Figure 8. After de pairing ($t = 38 - 44$) the spectrum reaches a law $E(k_x) \sim k_x^{-2}$ for wave numbers < 20 , as shows the segment of straight line of the Figure 8. For wave numbers between 20 and 30, is reached a small zone of law $E(k_x) \sim k_x^{-3}$, followed of a zone of exponential decline.

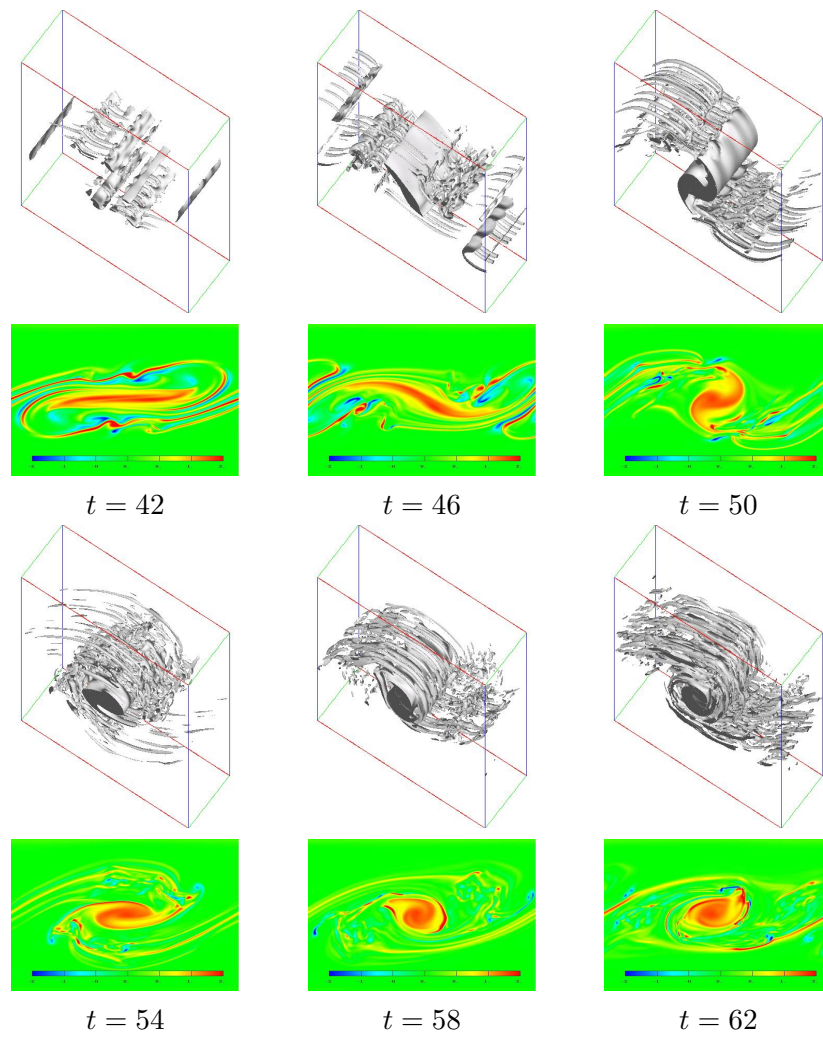


Figure 7: Isosurfaces of $Q = 0.2$ and streamwise cross-sectional plots of spanwise vorticity. Simulation 3DIII, $Re = 1000$, $Ri = 0.07$.

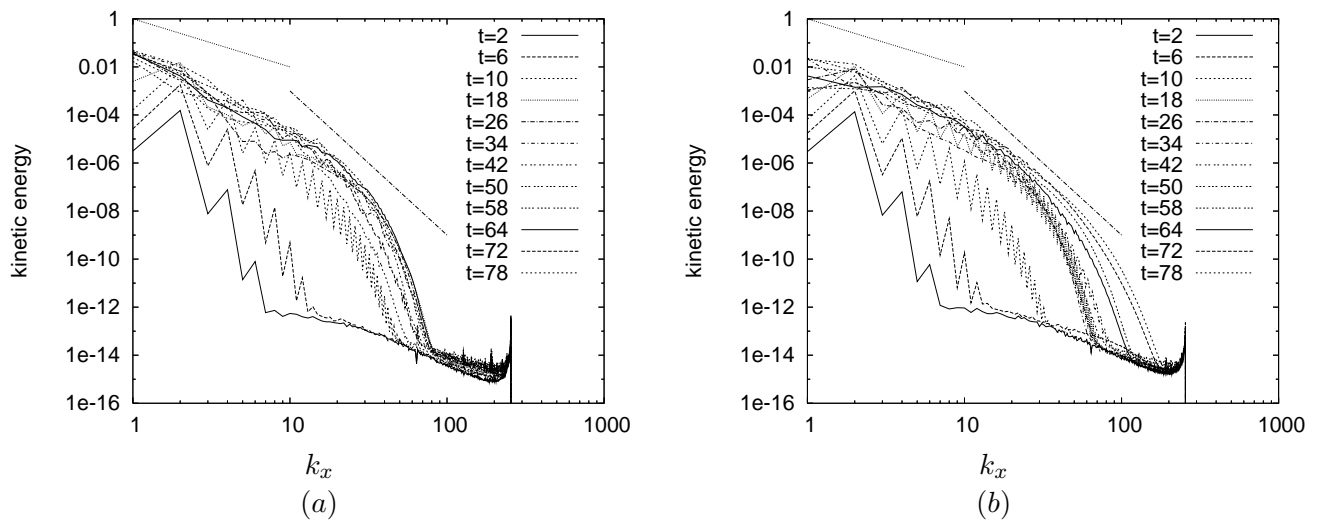


Figure 8: Spectrum of kinetic energy in function of the streamwise wave number at different times and $Re = 500$. (a) Simulation 3DI, $Ri = 0.07$, (b) Simulation 3DII, $Ri = 0.167$.

6 CONCLUSIONS

The purpose of the present work was to investigate the occurrence of secondary KH instability in the baroclinic layer of a three-dimensional stably stratified mixing layer and its influence in the formation of the streamwise vortices, using DNS. The numerical results showed that the intensity of the negative vorticity layer, generated between two co-rotating vortices, depends on the Richardson and Reynolds number and defines the occurrence or not of the secondary KH structures in the flow. We can conclude, based on the simulations presented in this work, that the calculation code employed solves the small scales and instabilities found in the baroclinic layer and that the resolution of the computational grids was chosen in agreement.

7 ACKNOWLEDGEMENTS

The authors wish to thank the CAPES-PICDT and CNPQ for sponsoring this project.

REFERENCES

- B. D. Altman. Critical layers in accelerating two-layer flows. *J. Fluid Mech.*, 197:429–451, 1988.
- P. Atsavapranee and M. Gharib. Structures in stratified plane mixing layers and the effects of cross-shear. *J. Fluid Mech.*, 342:53–86, 1997.
- C. P. Caulfield and W. R. Peltier. The anatomy of the mixing transition in homogenous and stratified free shear layers. *J. Fluid Mech.*, 413:1–47, 2000.
- G. M. Corcos and F. S. Sherman. Vorticity concentration and the dynamics of unstable free shear layers. *J. Fluid Mech.*, 73:241–264, 1976.
- A. B. Cortesi, G. Yadigaroglu, and S. Banerjee. Numerical investigation of the formation of three-dimensional structures in stably-stratified mixing layers. *Phys. Fluids*, 10:1449–1473, 1998.
- E. E. Gossard, J. H. Richter, and D. Atlas. Internal waves in the atmosphere from high-resolution radar measurements. *J. Geophys. Res.*, 75:3523–3535, 1970.
- L. R. Hauray, M. G. Briscoe, and M. H. Orr. Tidally generated internal wave packets in Massachusetts bay. *Nature*, 278:312–317, 1979.
- P. Hazel. Numerical studies of the stability of inviscid stratified shear flows. *J. Fluid Mech.*, 51:39–61, 1972.
- L. N. Howard. Note on a paper of John W. Miles. *J. Fluid Mech.*, 10:509–512, 1961.
- G. P. Klaassen and W. R. Peltier. The influence of stratification on secondary instability in free shear layers. *J. Fluid Mech.*, 227:71–106, 1991.
- S. Lardeau, E. Lamballais, and J. P. Bonnet. Direct numerical simulations of a jet controlled by fluid injection. *J. Turbulence*, 3:1–25, 2002.
- S. K. Lele. Compact finite difference schemes with spectral-like resolution. *J. Comp. Phys.*, 103:16–42, 1992.
- D. M. V. Martinez. *Transição à Turbulência na Camada de Mistura Estavelmente Estratificada utilizando Simulação Numérica Direta e Simulação de Grandes Escalas*. PhD thesis, Universidade Federal do Rio Grande do Sul, Brasil, 2006.
- D. M. V. Martinez, E. B. C. Schettini, and J. H. Silvestrini. Transition to turbulence in a stable stratified temporal mixing layer through direct numerical simulation. In *Proceedings of the 10th Congress of Thermal Sciences and Engineering*, page 9, Rio de Janeiro, RJ, Brazil, 2004.
- D. M. V. Martinez, E. B. C. Schettini, and J. H. Silvestrini. Secondary Kelvin-Helmholtz in-

- stability in a stably stratified temporal mixing layer. In *Proceedings of the 18th Congress of Mechanical and Engineering*, volume -, page 8, Ouro Preto, Brazil, 2005.
- D. M. V. Martinez, E. B. C. Schettini, and J. H. Silvestrini. The influence of stable stratification on the transition to turbulence in a temporal mixing layer. *J. of Braz. Soc. of Mech. Sci. and Eng.*, XXVIII:230–240, 2006.
- A. Michalke. On the inviscid instability of the hyperbolic tangent velocity profile. *J. Fluid Mech.*, 19:543–556, 1964.
- J. W. Miles. On the stability of heterogeneous shear flows. *J. Fluid Mech.*, 10:496–508, 1961.
- R. T. Pierrehumbert and S. E. Widnall. The two and three-dimensional instabilities of a spatially periodic shear flows. *J. Fluid Mech.*, 114:59–82, 1982.
- D. G. Showalter, C. W. Van Atta, and J. C. Lasheras. A study of streamwise vortex structure in a stratified shear layer. *J. Fluid Mech.*, 281:247–291, 1994.
- J. H. Silvestrini and E. Lamballais. Direct numerical simulations of wakes with virtual cylinders. *Int. J. Comp. Fluid Dyn.*, 16 (4):305–314, 2002.
- W. D. Smyth. Dissipation range geometry and scalar spectra in sheared, stratified turbulence. *J. Fluid Mech.*, 401:209–242, 1999.
- W. D. Smyth. Secondary Kelvin-Helmholtz instability in weakly stratified shear flow. *J. Fluid Mech.*, 497:67–98, 2003.
- C. Staquet. Two-dimensional secondary instabilities in a strongly stratified shear layer. *J. Fluid Mech.*, 296:73–126, 1995.
- C. Staquet. Mixing in a stably stratified shear layer: two and three-dimensional numerical experiments. *Fluid Dynamics Research*, 27:367–404, 2000.
- A. Thorpe. Laboratory observations of secondary structures in Kelvin-Helmholtz billows and consequences for ocean mixing. *Geophys. Astrophys. Fluid Dyn.*, 34:175–199, 1985.
- J. H. Williamson. Low-storage Runge-Kutta schemes. *J. Comp. Phys.*, 35:48, 1980.